European Journal of Nuclear Medicine and Molecular Imaging
https://doi.org/10.1007/s00259-019-04552-9

ORIGINAL ARTICLE

The role of additional late PSMA-ligand PET/CT in the differentiation between lymph node metastases and ganglia

Ian Alberts[1] · Christos Sachpekidis[1] · Lotte Dijkstra[1] · George Prenosil[1] · Eleni Gourni[1] · Silvan Boxler[2] · Tobias Gross[2] · George Thalmann[2] · Kambiz Rahbar[3] · Axel Rominger[1] · Ali Afshar-Oromieh[1]

Received: 20 June 2019 / Accepted: 24 September 2019

Abstract

Purpose Differentiating between prostate cancer (PC) lesions and benign structures which exhibit radiotracer uptake in PSMA-ligand PET/CT can be challenging. Additional late imaging has been shown to be a powerful method for the discrimination between PC and non-PC lesions, owing to the increasing tracer uptake of the former. Nevertheless, there are no pre-existing studies which describe the dynamic tracer uptake for ganglia, which this present study aims to address.

Methods Fifty consecutive patients with PC who received standard and late ^{68}Ga-PSMA-11-PET/CT (by local protocol at 1.5 h "standard" and 2.5 h p.i. "late") underwent retrospective evaluation. All lesions with a tracer uptake above local background indicative for ganglia as well as PC lesions were analysed with regard to their maximum standardised uptake values (SUVmax) and localisation.

Results Overall, 86 PSMA-positive ganglia were identified in 70% ($n = 35$) of the patients. Five ganglia exhibited PSMA avidity at late imaging only, and three at standard imaging only. A total of 66 lesions suggestive for PC were detected in 44 patients (88%), of which 45% ($n = 30$) were morphologically identified as lymph nodes (LN), the remainder being locally recurrent lesions or bone metastases. No solid organ metastases were present in our cohort. At late scanning, 73% of the LN exhibited an increase in SUVmax, whereas 65% of the ganglia exhibited a decreasing or stable SUVmax.

Conclusion Whereas the presence of increasing tracer uptake in potential PC lesions can provide additional data about the likelihood of malignancy, increasing SUVmax alone does not reliably differentiate between ganglia and PC lesions and is a potential diagnostic pitfall. We therefore recommend high-resolution CT to enable morphological characterisation of ganglia.

Keywords Prostate cancer · PET/CT · Positron emission tomography · PSMA · Prostate-specific membrane antigen · Ganglion

Introduction

Prostate cancer (PC) is the most common malignancy in men, and the third leading cause of cancer-related death in men [1]. Despite initial treatment, biochemical recurrence is a commonly encountered entity and presents a challenge for conventional imaging modalities given their limited abilities to detect disease at early stages of recurrence where the likelihood of salvage therapy being curative is greater.

The prostate-specific membrane antigen (PSMA), also known as folate hydrolase I or glutamate carboxypeptidase II, has become the focus of much attention owing to its high levels of expression on PC cells [2]. Following its clinical introduction in 2011, PSMA-ligand molecular imaging has rapidly established itself as the investigation of choice in recurrent PC [3–6]. Furthermore, PSMA-directed radioligand therapy is a rapidly evolving treatment modality for metastatic disease, creating a theragnostic role for PSMA-ligand molecular imaging [7].

Despite its name, PSMA expression is not limited to PC cells, but is observed in a wide variety of tissues, both pathological and physiological. For example, it has been

This article is part of the Topical Collection on Oncology – Genitourinary

✉ Ian Alberts
ian.alberts@insel.ch

[1] Department of Nuclear Medicine, Bern University Hospital, Freiburgstrasse 18, 3010 Bern, Switzerland

[2] Department of Urology, Bern University Hospital, Bern, Switzerland

[3] Department of Nuclear Medicine, University Hospital Münster, Münster, Germany

Published online: 21 December 2019

demonstrated that PSMA is expressed by the neovasculature of a wide variety of solid tumours [8]. Physiological PSMA expression is reported in the lacrimal and salivary glands, the liver, the spleen, the kidneys and the intestines [9]. PSMA-ligand uptake has also been observed in benign mediastinal lymph nodes. Such non-specific causes of tracer uptake create potential pitfalls when interpreting images [10]. Furthermore, numerous publications have demonstrated PSMA-avid peripheral nerve ganglia [11–15], with physiological PSMA expression reported to occur in astroglial cells [16], and is implicated in a number of neuropsychiatric disorders along with its homologue glutamate carboxypeptidase III [17, 18]. The factors that influence PSMA-ligand avidity for ganglion remain to be determined and are likely manifold.

A challenge for the nuclear medicine physician is therefore differentiating between genuine manifestations of PC and physiological, incidental radiotracer uptake in peripheral ganglia. The result is potential diagnostic confusion and could result in the incorrect staging of a patient's PC. To mitigate against this, a number of stratagems have been proposed: careful anatomic correlation [13] and examination of the lesion's configuration (with "band-shaped" being associated with ganglia and lymph-nodes being associated with "teardrop" or "nodular" morphologies [15]). Previous studies report that the intensity of uptake in ganglia is mild to moderate when compared with histologically confirmed lymph node (LN) metastases [15]. The pattern of radiotracer uptake may also be useful: PC metastases are associated with increasing tracer uptake over time [9, 10, 19, 20]. Equivocal cases might therefore be resolved by considering the pattern of uptake in biphasic imaging [19]. However, to our knowledge, hitherto there have been no reports describing the dynamic patterns of uptake for PSMA-ligands in ganglia, which this present study aims to address.

Materials and methods

In this retrospective analysis, we investigated 50 individuals (characteristics outlined in Table 1) with biochemically recurrent PC who were referred to our centre for ^{68}Ga-PSMA-11-PET/CT between 11/2018 and 02/2019. Imaging was performed at 1.5 h post injection of radiotracer (p.i.) with additional late scanning performed at 2.5h p.i. Since numerous publications have shown the advantages of later scanning in PSMA-imaging [9, 19, 21–23], we modified our standard scanning protocol from 1 h p.i. to 1.5 h p.i. in January 2018 (the protocol is further detailed in the following paragraph). At our centre, the decision to carry out late scans is a clinical judgement and is primarily employed in order to clarify unclear findings at standard scanning or to increase the probability of tumour detection in cases of negative standard scans, and is standard of care in our institution. Due to the retrospective nature of the analysis, it is not possible to reconstruct the particular situations (which are individual to each case) in which the decision was made to conduct an additional late scan. The majority of patients (n = 34) had undergone initial operative treatment by radical prostatectomy. Two received radiotherapy as initial management alone, and seven underwent combined operative and radiotherapy. Complete details of initial therapy were not available in the clinical notes of seven patients. Further details regarding age, Gleason score, initial staging, applied activity and the prostate-specific antigen (PSA) value at time of scanning are as outlined in Table 1.

Radiotracer

^{68}Ga-PSMA-11 was produced as previously described [6, 24]. In brief, $^{68}Ga^{3+}$ was obtained from a ^{68}Ge/^{68}Ga radionuclide generator and used for radiolabelling of PSMA-11. The ^{68}Ga-PSMA-11 solution was given by intravenous bolus injection (mean of 202 ± 35 MBq, range 124–280 MBq).

Imaging

All patients received regular whole body PET scans (from the head to the thighs) at 1.5 h p.i following peroral hydration with 1 L of water (beginning from 30 min p.i.) and 20 mg of i.v. Furosemide (at 1 h p.i.). Late imaging was performed at 2.5 h p.i. (from Xiphoid process to the thighs) with peroral hydration ad libitum. Both scans at 1.5 h and 2.5 h p.i. were analysed for pathological lesions characteristic for PC in addition to the presence of ganglia exhibiting increased radiotracer uptake relative to the local background.

Image acquisition

All patients were investigated using the same Biograph Vision PET/CT digital scanner (Siemens, Erlangen, Germany). A non-contrast-enhanced CT scan from pelvis to vertex was performed 1.5 h post tracer injection using the following parameters: slice thickness of 1.0 mm; pitch factor 1; soft tissue reconstruction kernel; maximum of 120 keV and 90 mAs by applying CARE kV and CARE Dose. Immediately after CT scanning, a whole body PET (pelvis to vertex) was acquired in 3D (matrix 440 × 440) with a zoom factor of 1.0. A total acquisition time of 20 min using flow-technology (0.7 mm/s table velocity) and an axial field of view (FOV) of 726 mm was used. The emission data were corrected for randoms, scatter and decay. Reconstruction was conducted with a TrueX + TOF algorithm and Gauss-filtered to a transaxial resolution of 2 mm at FWHM (full width at half maximum). Attenuation correction was performed using the low-dose non-enhanced computed tomography data. PET and CT were performed using the same protocol for every patient. 2.5 h after the tracer injection, an additional "late" PET/CT scan

Table 1 Patient characteristics (*PSA*, prostate specific antigen; *OP*, operative treatment; *RT*, radiotherapy)

Characteristic	Values
Age (mean/standard deviation/range/median)	68/19/54–84/68.5
Gleason score (range/median)	6–9/7
PSA (ng/ml) (mean/standard deviation/range/median)	9.03/22.2/0.03–105/1.3
Coeliac (mean/standard deviation/range/*p* value)	– 19%/15%/– 39%–12%/< 0.001
Initial therapy	34 × OP
	7 × OP + adj. RT
	2 × RT
Initial TNM	3 × T1, 15 × T2, 13 × T3, 11 × N1, 2 × Nx
Injected activity (MBq) (mean/standard deviation/range/median)	202/17.6/124–280/202

was performed from the pelvis to the upper abdomen (including the Xiphoid process) using a longer acquisition time (0.5 mm/s table velocity), otherwise with the same acquisition parameters as above.

Image evaluation

Image analysis was performed using an appropriate workstation and software (SyngoVia; Siemens, Erlangen, Germany). Two experienced physicians (one post-graduate physician with 7 years clinical experience and one board-certified nuclear physician with 14 years experience—first and last authors, respectively) read the data set together and resolved any disagreements by consensus. Lesions that were visually considered to be suggestive for PC or ganglia exhibiting increased tracer uptake relative to local background were counted and analysed with respect to their type (local relapses, lymph node, bones), localisation and to their maximum standardised uptake value (SUVmax) in, both the standard and late images. Ganglia were grouped according to anatomic location: presacral or coeliac plexus. The stellate and cervical plexus ganglions were not included in our routine late imaging and were therefore disregarded in this analysis.

For calculation of the SUVmax, circular regions of interest were drawn around areas with focally increased uptake in transaxial slices and automatically adapted to a three-dimensional volume of interest at a 40% isocontour as previously described [6]. Visual criteria for the differentiation between ganglia and lymph nodes were as described previously [15] (namely band shape, teardrop or nodular configuration) and was aided by a co-registered thin-slice CT (1-mm slice thickness). A maximum of five PC lesions and five ganglia were selected in patients with multiple PSMA-positive lesions in order to prevent over-representation of these individuals in our cohort thereby avoiding the introduction of possible bias. Only one patient was identified with more than five PSMA-positive ganglia and three patients had more than five PC lesions.

Measurement of the SUVmax at 1.5 h and 2.5 h allowed for a percentage change in tracer uptake to be obtained. Percentage changes between − 10 and + 10% were considered to be "stable", i.e. showing no significant change. Those greater than + 10% were considered to be "increasing" and those less than − 10% were considered to be "decreasing". Ten percent is a conservative estimate based on previously reported variability in SUV measurements [25, 26].

Statistical analysis

SUVmax values of the ganglia and PC lesions at 1.5 h and 2.5 h p.i. were compared using the paired Student's *t* test to evaluate differences between the standard and late images and the unpaired *t* test to evaluate differences between lesion types; a two-tailed *p* value of < 0.05 was considered statistically significant. To test for associations between lesion type and pattern of behaviour (increasing vs. stable/decreasing), Fisher's exact test was used. We evaluated the diagnostic utility of changes in SUVmax in the differential diagnosis of lymph nodes and ganglia by construction of a Punnett square, from which sensitivity and specificity can be derived. Finally, associations between ganglion tracer uptake and PET positivity were considered. To test for an association between PET positivity and ganglion frequency, Fisher's exact test was used. The unpaired *t* test was used to evaluate differences between SUVmax at 1.5 and 2.5 h and the magnitude of SUVmax change for the PSMA positive and PSMA negative groups.

Results

PC lesions

In our cohort of 50 patients, 66 lesions characteristic for PC were identified in the 44 patients (88% of the patient cohort) and 86 lesions characteristic of ganglia were identified in a total of 35 patients (70% of the patient cohort). Six patients (12%) had no identifiable pathological lesions (negative PET). All lesions had clear computer tomographic correlates, and all were identified as PET positive in both standard and late

imaging. Of the PC lesions, 30 were identified as lymph nodes, 25 lesions of locally recurrent PC (in the prostatic fossa and seminal vesicles) and 11 bone metastases.

Measuring SUVmax at 1.5 h ("standard") and 2.5 h ("late"), we obtained increased SUVmax at late imaging, with statistically significant differences between standard and late imaging ($p = 0.009$). We then grouped all PC lesions by "increasing", "stable" and "decreasing" SUVmax as shown in Fig. 1. The majority of PC lesions exhibited increasing tracer uptake (73%), with 15% remaining "stable" and 12% showing decreasing tracer uptake. Of the 30 PSMA-positive lymph nodes, 22 exhibited increasing tracer uptake (73%), with the remaining eight being either stable or decreasing.

Ganglia

A total of 86 PSMA-positive ganglia were identified in 35 patients (70%), with a total of 50 ganglia in the pre-sacral plexus and 36 in the coeliac plexus being identified; all lesions included had clear computed tomographic correlates. Example images for coeliac (Fig. 2) ganglia are depicted.

We observed a heterogeneous pattern of tracer uptake for the ganglia. In the PET images on visual analysis, three ganglia exhibited PSMA positivity on standard imaging only (and not visible in the late images) and eight were identifiable only at late imaging. Using the same method as above, we obtained values for SUVmax. In contrast between ganglia types (coeliac versus pre-sacral), the coeliac ganglia were associated with a statistically significant higher tracer uptake at standard uptake ($p = 0.003$) and higher (albeit non-significant) tracer uptake at late imaging ($p = 0.12$). The results are shown in Table 2. The ganglia were then grouped according to the direction of change, with roughly half of the ganglia exhibiting a decreasing tracer uptake (45%), the remainder presenting with either stable (21%) or increasing (34%) tracer uptake.

Patterns of uptake in PC lesions and ganglia

As shown in Fig. 3, a significantly ($p < 0.001$) higher tracer uptake at both standard and late imaging was observed in PC lesions when compared with both groups of ganglia (coeliac and pre-sacral). The absolute SUVmax values are listed in Table 2.

We then considered the dynamic behaviour of ganglia compared with lymph node metastases of PC. Whereas the lymph node metastases demonstrated a statistically significant higher tracer uptake at late imaging in comparison with standard imaging ($p < 0.001$), the ganglia were not associated with statistically significant change in SUVmax values ($p = 0.4$ for coeliac ganglia and $p = 0.6$ for pre-sacral ganglia), demonstrating their largely stable and heterogeneous pattern of behaviour.

Lesions identified as lymph nodes or ganglia based on CT imaging were then classified according to increasing, decreasing or stable SUVmax in the late images (i.e. positive or stable/negative percentage change from standard to late imaging, as described); the results are shown in the histogram found in Fig. 4.

We then considered whether the presence of rising tracer uptake acts as a potential diagnostic criterion to distinguish between lymph node metastasis of PC and ganglia. Using the morphological classification as the lesions in the thin-slice CT as the benchmark, a Punnett square for the observed frequencies of rising and falling tracer uptake can be constructed (Fig. 5). Correspondingly, the diagnostic accuracy of the finding of increasing SUVmax (defined as [true positives + true negatives] ÷ total population) yields 67%, with a relatively high sensitivity (73%) and moderate specificity (65%). Although the positive predictive value of increasing tracer uptake is low (42%), its absence has a high negative predictive value (88%). We then used Fisher's exact test to consider the association

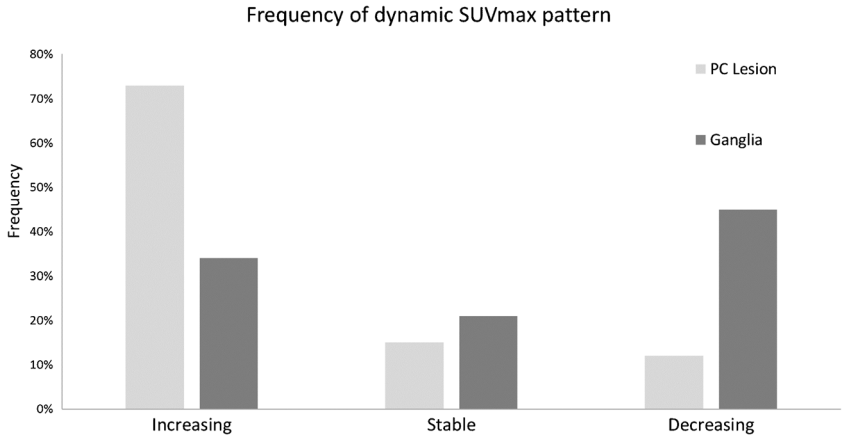

Fig. 1 Direction of change in SUVmax for both ganglia and PC lesions from "standard" to "late" imaging

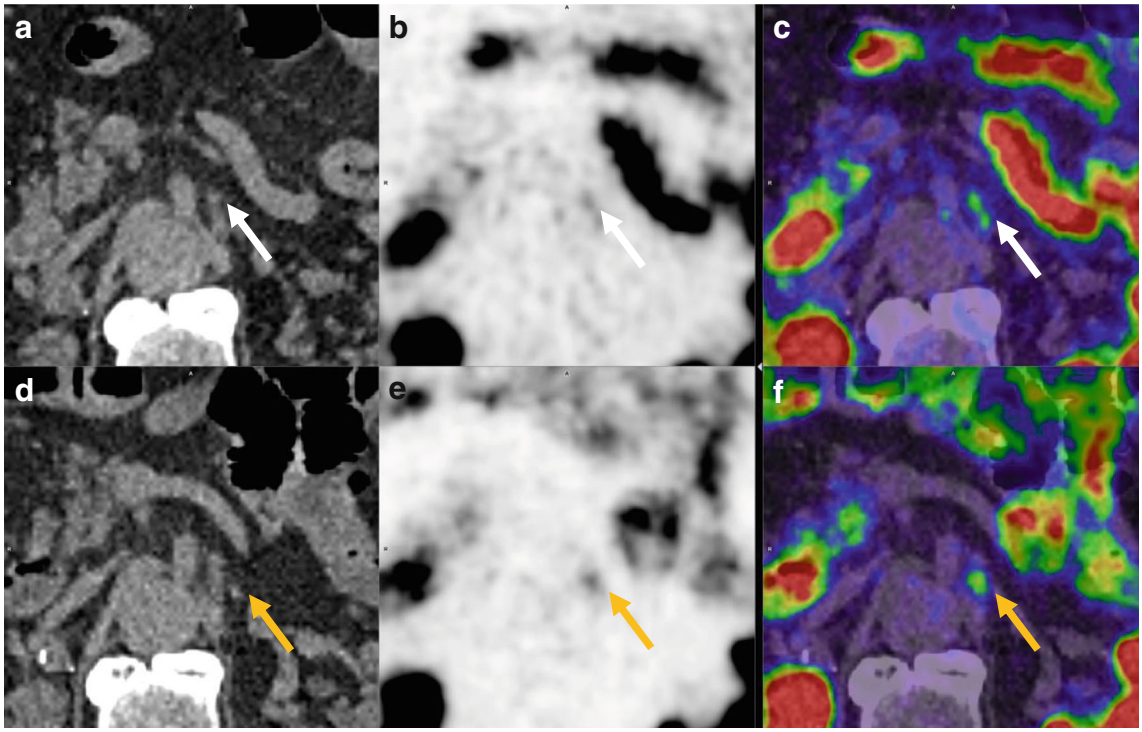

Fig. 2 Coronal images showing example of PSMA-positive ganglia in the coeliac plexus. The focal, increased tracer uptake in the standard images (indicated by yellow arrows at the bottom row) could easily be mistaken for a PC lesion. The late images (top row) show barely increased tracer uptake beyond background. In the CT, the typical filiform pattern associated with ganglia can be discerned. The two CT images (A,D) show a long, filiform object which correlates to a ganglion. (Tiles D,E,F standard images; tiles A,B,C late images; tiles A,D CT images; tiles B,E PET; tiles C,F fusion of PET and co-registered CT)

between rising tracer uptake and lesion type (ganglia and lymph nodes), giving a two-tailed $p < 0.001$.

Finally, an intra-patient analysis of the patterns of tracer uptake revealed heterogeneous patterns of uptake with three predominant visual patters observed: increasing, decreasing and discordant. For the latter, patterns of concomitantly increasing and decreasing tracer activity were seen to occur in paired structures, as exemplified by the pair of sacral plexus ganglia presented in Fig. 6. Such a discordant pattern was observed in 17 of the patients (49%), further highlighting the heterogeneous pattern of tracer uptake.

Table 2 SUVmax values at standard and late imaging for coeliac, sacral and PC lesions. *Min*, minimum; *Max*, maximum; *SD*, standard deviation

Parameter	Coeliac		Pre-sacral		PC lesions	
	Standard	Late	Standard	Late	Standard	Late
Mean	3.77	3.4	2.8	2.8	16.8	19.7
Min–max	2.0–7.5	1.2–10.8	1.1–7.4	1.5–7.6	2.0–75.4	2.0–89.7
SD	1.4	2.1	1.2	1.1	16.5	17.9
Median	3.4	2.9	2.6	2.6	11	14

Association with PET positivity

We considered the potential for PET positivity as a confounder. No significant association between PET positivity and ganglion frequency was observed. Furthermore, no association between PET positivity or negativity and the SUVmax at 1.5 h, 2.5 h or the magnitude and direction of change was observed.

Discussion

Numerous studies have highlighted the unspecific nature of PSMA expression, with ganglia representing a potential diagnostic pitfall [11, 13]. With new generation digital PET/CT scanners reporting ever higher sensitivity and resolution [27], such small yet PSMA-avid lesions are likely to present an increasing diagnostic challenge for nuclear medicine physicians. The new paradigm of theragnostics makes the accurate staging and identification of PSMA-avid lesions yet more important, as well as raising questions about the potential for side effects arising from both physiological and pathological PSMA expression [28]. It is with this in mind that we sought to investigate the dynamic radiopharmaceutical uptake for ganglia using ^{68}Ga-PSMA-11-PET. To our knowledge, this

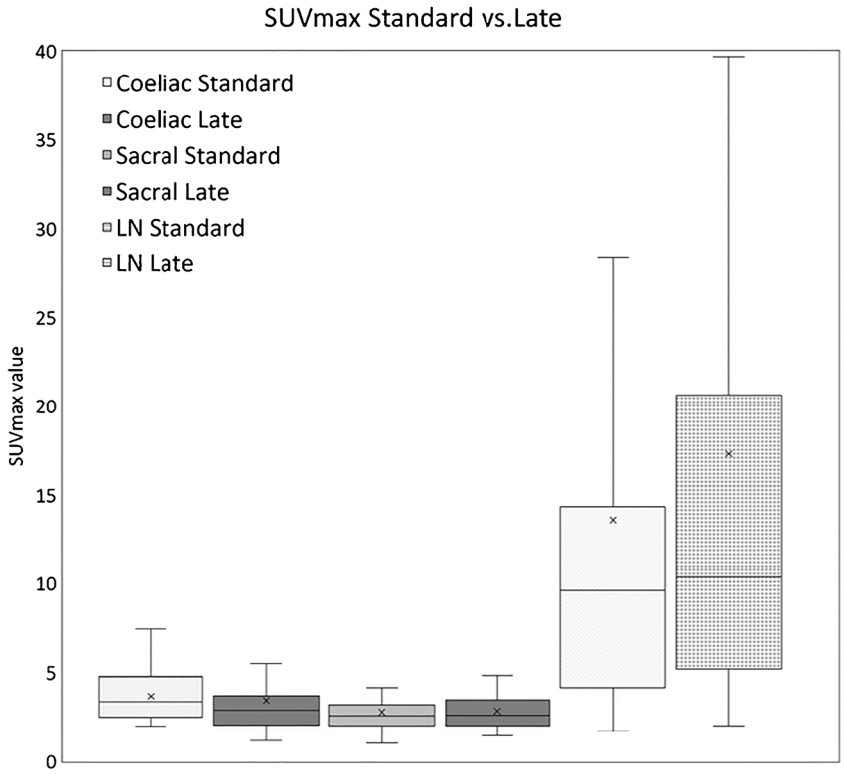

Fig. 3 Box and whisker plots showing SUVmax at standard and late imaging respectively for both coeliac (left) and sacral (middle) as well as PSMA-positive lymph nodes (LN) (right). Cross = median, line = mean, whisker = max/min. Significantly higher SUVmax values were obtained for PC lesions compared with ganglia ($p > 0.001$)

is the first publication of this kind aiming to resolve this clinically relevant diagnostic question.

We identified PSMA-positive lesions characteristic of ganglia in 70% of our patients, broadly in keeping with detection rates quoted by Rischpler, who found in 89.4% of patients PSMA-positive coeliac plexus ganglia and in 49% sacral plexus ganglia [15]. We noted a statistically significant greater SUVmax in PC lesions (including lymph node metastases) compared with ganglia, which is in agreement with already published results [11, 15] and previous studies demonstrating association between intensity of tracer uptake and histopathological positivity for PC [29].

Nevertheless, as was demonstrated by the significant overlap in SUVmax values for lymph node metastases and ganglia, the two structures can easily be mistaken visually, and ganglia presented a higher SUV than previously suggested "cut-off" values for "PSMA positivity" (SUV > 2) [30]. Indeed, in a PET/MRI study of coeliac ganglia, Bialek and Malkowski reported that roughly 50% of patients presented with at least one coeliac ganglia which was confusable with a PSMA-positive lymph node either on grounds of size, shape or tracer uptake [31]. Compared with the pre-sacral ganglia, we recorded higher average SUVmax values in the coeliac ganglia, which was also in agreement with previous studies [15].

Whereas the physical half-life of the radioisotope (^{68}Ga) is short (68 min), previous studies have confirmed that ^{68}Ga-PSMA-11 exhibits an increase in tracer uptake over time in the majority of PC lesions [9, 10, 19, 20]. This favourable

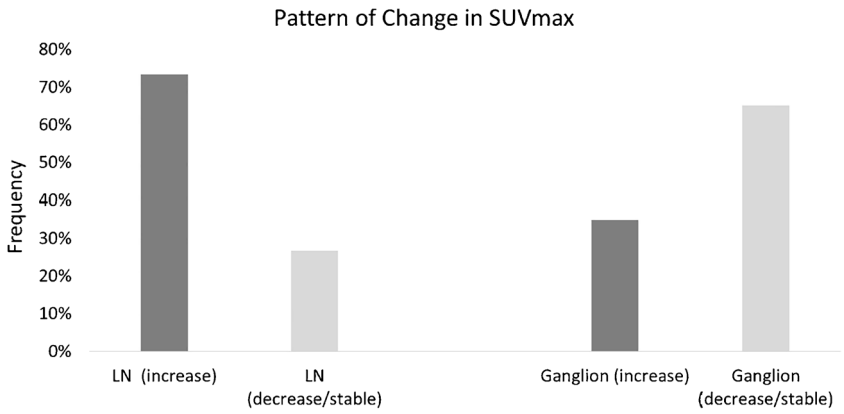

Fig. 4 Histograms of SUVmax change at standard and late imaging for PSMA-positive lymph nodes (LN) (left) and ganglia (right). Whereas the majority of lesions identified as lymph nodes (LN) exhibited an increasing SUVmax, the majority of ganglia demonstrated a decreasing or stable SUVmax

	Benchmark - CT		
	LN	Ganglion	
Increasing SUVmax	22	30	PPV: 42%
Decreasing SUVmax	8	56	NPV: 88%
	Sens: 73%	Spec: 65%	

Fig. 5 Punnett square for the observed frequencies of rising and falling tracer uptake in lymph nodes (LN) and ganglia. We assess the diagnostic performance of increasing SUVmax in distinguishing between lymph node (LN) lesions of PC and ganglia, using the thin-slice CT as the benchmark. We see from this Punnett square that while increasing values of SUVmax has low specificity in distinguishing LN from ganglia, its absence has a high negative predictive value in ruling out potential LN metastases. *PPV*—Positive predictive value, *NPV*—Negative predictive value, *Sens*—Sensitivity, *Spec*—Specificity. "Decreasing" SUVmax defined as falling or stable (– 10% < SUV > + 10%)

pharmacokinetic property means that in cases of diagnostic uncertainty (for example in distinguishing between pathological and non-pathological tracer uptake for a lymph node), the pattern of tracer uptake in late imaging has been posited as providing useful diagnostic information [9]. This paradigm is supported by our observation that a statistically significant increase in SUVmax at late imaging was observed in PC lesions (73% of which exhibit increase).

In contrast, the ganglia were not associated with a statistically significant increased tracer uptake at late imaging. However, we interpret this finding with caution. Given that roughly a third of ganglia exhibited increased tracer uptake (the remaining exhibited stable or decreasing patterns). We therefore conclude that this criterion clearly cannot be used reliably to differentiate between lesion types (ganglia vs. lymph node metastases). Indeed, this notion finds support in our statistical analysis. Although Fisher's exact test did reveal an association between these two lesion types and the characteristic of increased tracer uptake which reached statistical significance, analysis of the diagnostic performance of rising tracer uptake using CT categorisation of the lesions yielded a low diagnostic accuracy (67%), albeit with a relatively high negative predictive value (NPV) of 88%. We interpret this high NPV as meaning that in ambiguous cases, the absence of rising tracer uptake potentially provides useful diagnostic information as a rule-out criterion, whereas rising SUVmax should be regarded as unspecific when considering the differential diagnosis of ganglia versus lymph nodes.

Reviewing the previous literature, we note that in several works complete PET/CT examination parameters were not recorded. In other studies, we note the use of CT slice thicknesses of 5mm and filters with a full width half maximum (FWHM) of 5mm, which are limitations imposed by the performance characteristics of the previous generation of PET detectors. We draw attention to the well-known partial volume effect, and the fact that the PET/CT resolution in such studies is likely larger than

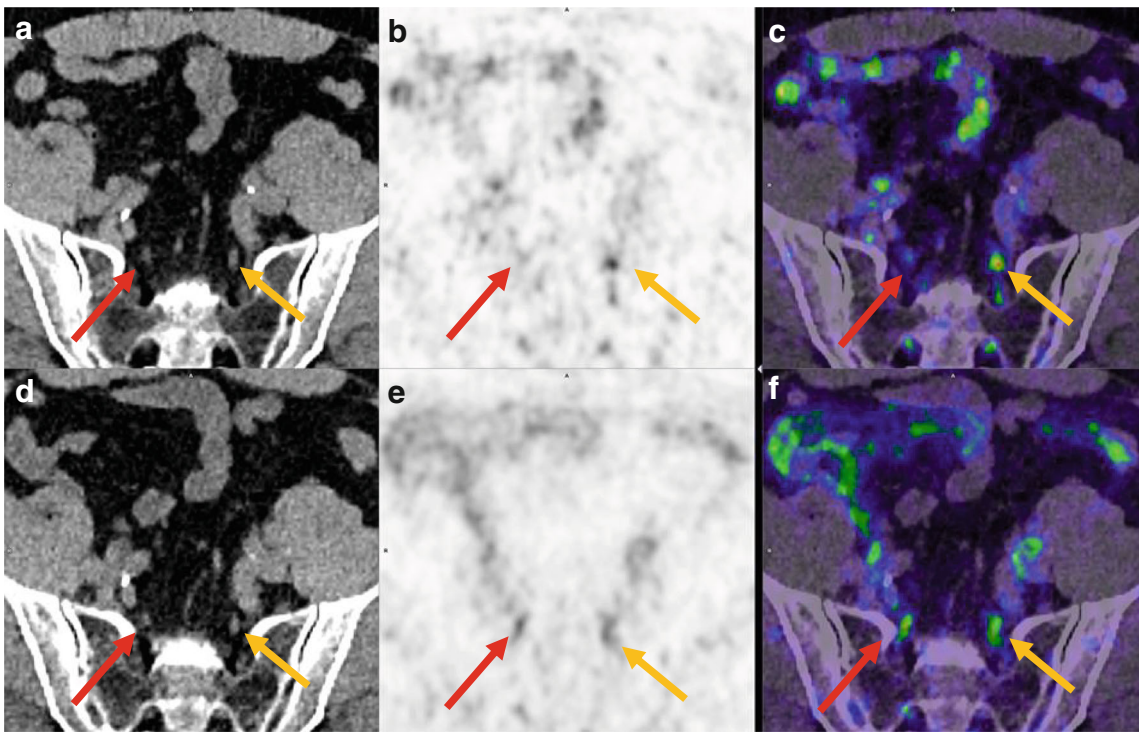

Fig. 6 Discordant tracer uptake in a pair of sacral ganglia. Whereas the left ganglion (yellow arrow) exhibits visually increased uptake in late imaging, the right ganglion (red arrow) shows barely increased tracer uptake beyond background in the late imaging (Left: SUVmax standard 2.7, SUVmax late 4.8; Right: SUVmax standard 3.2, SUVmax late 2.0). Tiles D,E,F standard images, tiles A,B,C late images; tiles A,D CT images; tiles B,E PET; tiles C,F fusion of PET and co-registered CT

the cross-sectional diameter of most ganglia (reported to be 3 mm ± 1 mm in cadaveric studies [32]). Furthermore, previous studies demonstrate the influence of voxel size upon the measured SUVmax, of the choice of reconstruction algorithm in the detectability of ganglia and the positron range for the various radionuclides (mean positron range in soft tissue ^{18}F 0.27 mm; ^{68}Ga 1.05 mm), which place physical limits upon the maximum resolution obtainable [33–35]. We therefore interpret quantitative tracer uptake analyses in such studies with a high degree of caution.

In this present study, we employed a PET scanner with favourable performance characteristics (reported spatial resolution at FWHM and 1 cm from centre of FOV of 3.6 mm) [36], which we argue better enables the quantification of such small lesions and is potentially less vulnerable to the limitations described above, particularly the partial volume effect. Nevertheless, until the new generation of digital PET/CT scanners which are currently being brought into the market by various manufacturers become widely adopted in routine clinical use, the authors advise caution in using patterns of tracer uptake to differentiate between PC lesions and ganglia. Instead, we draw attention to the thin-slice size in our CT protocol (1 mm) which aids considerably the detection, identification and morphological characterisation of such small structures. Therefore, based on these findings, we strongly recommend the routine use of CT protocols which enable the reconstruction of thin slices to support differential diagnosis of PSMA-positive lesions at standard imaging. In cases which remain unclear, additional late imaging can be performed, where the absence of increasing SUVmax can be of additional diagnostic use in the differentiation of ganglia from PC lesions.

As described above, the positron range of ^{18}F is shorter than that of ^{68}Ga, resulting in potentially higher spatial resolution. As a result, ^{18}F-PSMA ligands are reported to exhibit a higher detection efficiency [37], and consequently it is widely reported that artefactual tracer uptake in small lesions such as ganglia is even greater. We therefore assume that with the increasing adoption of ^{18}F-PSMA ligands, our present findings will be of even greater relevance when considering the potential for false positives resulting in over-diagnosis, and urge that our recommendations be borne in mind when considering new study protocols.

In this retrospective study, our patients were referred for staging of biochemical recurrence and largely went on either to conservative or palliative management, salvage radiotherapy or chemotherapy. Although there was no histological correlation, the thin-slice CT protocol of our high performance 3rd generation digital PET/CT scanner enabled a reliable morphologic differentiation between ganglia and lymph nodes. We note numerous studies confirming the high specificity of PSMA, such as that of Perera et al [38]. We also note that our patient cohort who all received additional late imaging for indeterminate feature may represent a source of bias. Studies of prospective design are required to address this limitation.

Conclusion

While the majority of PC lesions exhibit an increasing tracer uptake, one-third of the coeliac and pre-sacral ganglia also presented with increasing uptake values. Therefore, the observation of increasing SUV values alone cannot reliably help to differentiate ganglia from lymph node metastases of PC although the absence of rising SUV has a high negative predictive value in ruling out PC lesions. Although the uptake in ganglia was significantly lower compared with lymph node metastases, there is a remarkable overlap of the SUV values, meaning that absolute SUV value alone cannot be a reliable criterion to differentiate the two lesion types; relying on uptake patterns alone therefore represents a potential diagnostic pitfall.

According to the first description of dynamic patterns of radiotracer uptake in ganglia and to our experiences, we recommend conducting thin-slice CT scans which can better show the characteristic morphology of ganglia (such as band or teardrop shape), and can more reliably identify ganglia compared with quantitative analysis of SUV values.

Compliance with ethical standards

Conflicts of interest The authors declare that they have no conflict of interest.

Ethical approval All patients published in this manuscript signed a written informed consent form for the purpose of anonymized evaluation and publication of their data. This evaluation was approved by the ethics committee of the University of Bern (KEK-Nr. 2018-00299).

References

1. Siegel RL, Miller KD, Jemal A. Cancer statistics, 2017. CA Cancer J Clin. 2017;67:7–30. https://doi.org/10.3322/caac.21387.
2. Israeli RS, Powell CT, Corr JG, Fair WR, Heston WDW. Expression of the prostate-specific membrane antigen. Cancer Res. 1994;54:1807.
3. Afshar-Oromieh A, Zechmann CM, Malcher A, Eder M, Eisenhut M, Linhart HG, et al. Comparison of PET imaging with a (68)Ga-labelled PSMA ligand and (18)F-choline-based PET/CT for the diagnosis of recurrent prostate cancer. Eur J Nucl Med Mol Imaging. 2014;41:11–20. https://doi.org/10.1007/s00259-013-2525-5.
4. Afshar-Oromieh A, Holland-Letz T, Giesel FL, Kratochwil C, Mier W, Haufe S, et al. Diagnostic performance of 68Ga-PSMA-11 (HBED-CC) PET/CT in patients with recurrent prostate cancer: evaluation in 1007 patients. Eur J Nucl Med Mol Imaging. 2017;44:1258–68. https://doi.org/10.1007/s00259-017-3711-7.
5. Eiber M, Maurer T, Souvatzoglou M, Beer AJ, Ruffani A, Haller B, et al. Evaluation of hybrid (6)(8)Ga-PSMA ligand PET/CT in 248 patients with biochemical recurrence after radical prostatectomy. J Nucl Med. 2015;56:668–74. https://doi.org/10.2967/jnumed.115.154153.
6. Afshar-Oromieh A, Avtzi E, Giesel FL, Holland-Letz T, Linhart HG, Eder M, et al. The diagnostic value of PET/CT imaging with

the (68)Ga-labelled PSMA ligand HBED-CC in the diagnosis of recurrent prostate cancer. Eur J Nucl Med Mol Imaging. 2015;42:197–209. https://doi.org/10.1007/s00259-014-2949-6.
7. Virgolini I, Decristoforo C, Haug A, Fanti S, Uprimny C. Current status of theranostics in prostate cancer. Eur J Nucl Med Mol Imaging. 2018;45:471–95. https://doi.org/10.1007/s00259-017-3882-2.
8. Chang SS. Overview of prostate-specific membrane antigen. Rev Urol. 2004;6:S13–S8.
9. Afshar-Oromieh A, Malcher A, Eder M, Eisenhut M, Linhart HG, Hadaschik BA, et al. PET imaging with a [68Ga]gallium-labelled PSMA ligand for the diagnosis of prostate cancer: biodistribution in humans and first evaluation of tumour lesions. Eur J Nucl Med Mol Imaging. 2013;40:486–95. https://doi.org/10.1007/s00259-012-2298-2.
10. Afshar-Oromieh A, Sattler LP, Steiger K, Holland-Letz T, da Cunha ML, Mier W, et al. Tracer uptake in mediastinal and paraaortal thoracic lymph nodes as a potential pitfall in image interpretation of PSMA ligand PET/CT. Eur J Nucl Med Mol Imaging. 2018;45:1179–87. https://doi.org/10.1007/s00259-018-3965-8.
11. Krohn T, Verburg FA, Pufe T, Neuhuber W, Vogg A, Heinzel A, et al. [(68)Ga]PSMA-HBED uptake mimicking lymph node metastasis in coeliac ganglia: an important pitfall in clinical practice. Eur J Nucl Med Mol Imaging. 2015;42:210–4. https://doi.org/10.1007/s00259-014-2915-3.
12. Werner RA, Sheikhbahaei S, Jones KM, Javadi MS, Solnes LB, Ross AE, et al. Patterns of uptake of prostate-specific membrane antigen (PSMA)-targeted (18)F-DCFPyL in peripheral ganglia. Ann Nucl Med. 2017;31:696–702. https://doi.org/10.1007/s12149-017-1201-4.
13. Kanthan GL, Hsiao E, Vu D, Schembri GP. Uptake in sympathetic ganglia on 68Ga-PSMA-HBED PET/CT: a potential pitfall in scan interpretation. J Med Imaging Radiat Oncol. 2017;61:732–8. https://doi.org/10.1111/1754-9485.12622.
14. Hubble D, Robins P. RE: Uptake in sympathetic ganglia on 68Ga-PSMA-HBED PET/CT: a potential pitfall in scan interpretation. J Med Imaging Radiat Oncol. 2018;62:377–8. https://doi.org/10.1111/1754-9485.12739.
15. Rischpler C, Beck TI, Okamoto S, Schlitter AM, Knorr K, Schwaiger M, et al. (68)Ga-PSMA-HBED-CC uptake in cervical, coeliac and sacral ganglia as an important pitfall in prostate cancer PET imaging. J Nucl Med. 2018. https://doi.org/10.2967/jnumed.117.204677.
16. Berger UV, Luthi-Carter R, Passani LA, Elkabes S, Black I, Konradi C, et al. Glutamate carboxypeptidase II is expressed by astrocytes in the adult rat nervous system. J Comp Neurol. 1999;415:52–64. https://doi.org/10.1002/(SICI)1096-9861(19991206)415:1<52::AID-CNE4>3.0.CO;2-K.
17. Evans JC, Malhotra M, Cryan JF, O'Driscoll CM. The therapeutic and diagnostic potential of the prostate specific membrane antigen/glutamate carboxypeptidase II (PSMA/GCPII) in cancer and neurological disease. Br J Pharmacol. 2016;173:3041–79. https://doi.org/10.1111/bph.13576.
18. Hlouchová K, Bařinka C, Klusák V, Šácha P, Mlčochová P, Majer P, et al. Biochemical characterization of human glutamate carboxypeptidase III. J Neurochem. 2006;101:682–96. https://doi.org/10.1111/j.1471-4159.2006.04341.x.
19. Afshar-Oromieh A, Sattler LP, Mier W, Hadaschik BA, Debus J, Holland-Letz T, et al. The clinical impact of additional late PET/CT imaging with (68)Ga-PSMA-11 (HBED-CC) in the diagnosis of prostate cancer. J Nucl Med. 2017;58:750–5. https://doi.org/10.2967/jnumed.116.183483.
20. Sahlmann C-O, Meller B, Bouter C, Ritter CO, Ströbel P, Lotz J, et al. Biphasic 68Ga-PSMA-HBED-CC-PET/CT in patients with recurrent and high-risk prostate carcinoma. Eur J Nucl Med Mol Imaging. 2016;43:898–905. https://doi.org/10.1007/s00259-015-3251-y.
21. Afshar-Oromieh A, Hetzheim H, Kubler W, Kratochwil C, Giesel FL, Hope TA, et al. Radiation dosimetry of (68)Ga-PSMA-11 (HBED-CC) and preliminary evaluation of optimal imaging timing. Eur J Nucl Med Mol Imaging. 2016;43:1611–20. https://doi.org/10.1007/s00259-016-3419-0.
22. Afshar-Oromieh A, Hetzheim H, Kratochwil C, Benesova M, Eder M, Neels OC, et al. The theranostic PSMA ligand PSMA-617 in the diagnosis of prostate cancer by PET/CT: biodistribution in humans, radiation dosimetry, and first evaluation of tumor lesions. J Nucl Med. 2015;56:1697–705. https://doi.org/10.2967/jnumed.115.161299.
23. Fendler WP, Eiber M, Beheshti M, Bomanji J, Ceci F, Cho S, et al. (68)Ga-PSMA PET/CT: joint EANM and SNMMI procedure guideline for prostate cancer imaging: version 1.0. Eur J Nucl Med Mol Imaging. 2017;44:1014–24. https://doi.org/10.1007/s00259-017-3670-z.
24. Eder M, Neels O, Muller M, Bauder-Wust U, Remde Y, Schafer M, et al. Novel preclinical and radiopharmaceutical aspects of [68Ga]Ga-PSMA-HBED-CC: a new PET tracer for imaging of prostate cancer. Pharmaceuticals (Basel). 7:779–96. https://doi.org/10.3390/ph7070779.
25. Lodge MA. Repeatability of SUV in oncologic (18)F-FDG PET. J Nucl Med. 2017;58:523–32. https://doi.org/10.2967/jnumed.116.186353.
26. Osborne JR, Kalidindi TM, Punzalan BJ, Gangangari K, Spratt DE, Weber WA, et al. Repeatability of [(68)Ga]DKFZ11-PSMA PET scans for detecting prostate-specific membrane antigen-positive prostate cancer. Mol Imaging Biol. 2017;19:944–51. https://doi.org/10.1007/s11307-017-1091-9.
27. Schillaci O, Urbano N. Digital PET/CT: a new intriguing chance for clinical nuclear medicine and personalized molecular imaging. Eur J Nucl Med Mol Imaging. 2019. https://doi.org/10.1007/s00259-019-04300-z.
28. van Kalmthout L, Stam A, Gans R, Lam M. Visual deficit possibly caused by lutetium-177 PSMA treatment. BMJ Case Rep. 2018. https://doi.org/10.1136/bcr-2018-225508.
29. Fendler WP, Schmidt DF, Wenter V, Thierfelder KM, Zach C, Stief C, et al. 68Ga-PSMA PET/CT detects the location and extent of primary prostate cancer. J Nucl Med. 2016;57:1720–5. https://doi.org/10.2967/jnumed.116.172627.
30. Vinsensia M, Chyoke PL, Hadaschik B, Holland-Letz T, Moltz J, Kopka K, et al. (68)Ga-PSMA PET/CT and volumetric morphology of PET-positive lymph nodes stratified by tumor differentiation of prostate cancer. J Nucl Med. 2017;58:1949–55. https://doi.org/10.2967/jnumed.116.185033.
31. Bialek EJ, Malkowski B. Celiac ganglia: can they be misinterpreted on multimodal 68Ga-PSMA-11 PET/MR? Nucl Med Commun. 2019;40:175–84. https://doi.org/10.1097/MNM.0000000000000944.
32. Zhang XM, Zhao QH, Zeng NL, Cai CP, Xie XG, Li CJ, et al. The celiac ganglia: anatomic study using MRI in cadavers. AJR Am J Roentgenol. 2006;186:1520–3. https://doi.org/10.2214/AJR.04.1765.
33. Koopman D, van Dalen JA, Lagerweij MC, Arkies H, de Boer J, Oostdijk AH, et al. Improving the detection of small lesions using a state-of-the-art time-of-flight PET/CT system and small-voxel reconstructions. J Nucl Med Technol. 2015;43:21–7. https://doi.org/10.2967/jnmt.114.147215.
34. Krohn T, Birmes A, Winz OH, Drude NI, Mottaghy FM, Behrendt FF, et al. The reconstruction algorithm used for [(68)Ga]PSMA-HBED-CC PET/CT reconstruction significantly influences the number of detected lymph node metastases and coeliac ganglia. Eur J Nucl Med Mol Imaging. 2017;44:662–9. https://doi.org/10.1007/s00259-016-3571-6.

35. Sanchez-Crespo A, Andreo P, Larsson SA. Positron flight in human tissues and its influence on PET image spatial resolution. Eur J Nucl Med Mol Imaging. 2004;31:44–51. https://doi.org/10.1007/s00259-003-1330-y.
36. van Sluis JJ, de Jong J, Schaar J, Noordzij W, van Snick P, Dierckx R, et al. Performance characteristics of the digital Biograph Vision PET/CT system. J Nucl Med. 2019. https://doi.org/10.2967/jnumed.118.215418.
37. Giesel FL, Knorr K, Spohn F, Will L, Maurer T, Flechsig P, et al. Detection efficacy of (18)F-PSMA-1007 PET/CT in 251 patients with biochemical recurrence of prostate cancer after radical prostatectomy. J Nucl Med. 2019;60:362–8. https://doi.org/10.2967/jnumed.118.212233.
38. Perera M, Papa N, Christidis D, Wetherell D, Hofman MS, Murphy DG, et al. Sensitivity, specificity, and predictors of positive (68)Ga-prostate-specific membrane antigen positron emission tomography in advanced prostate cancer: a systematic review and meta-analysis. Eur Urol. 2016;70:926–37. https://doi.org/10.1016/j.eururo.2016.06.021.